On Estimating the Basin-Scale Ocean Circulation from Satellite Altimetry

Part 1.

Straightforward Spherical Harmonic Expansion

Chang-Kou Tai

Scripps Institution of Oceanography

A-030

La Jolla, CA 92092

ABSTRACT

Direct estimation of the absolute dynamic topography from satellite altimetry has been confined to the largest scales (basically the basin-scale) owing to the fact that the signal-to-noise ratio is more unfavorable everywhere else. But even for the largest scales, the results are contaminated by the orbit error and geoid uncertainties. Recently a more accurate earth gravity model (GEM-T1) became available, thus giving us the opportunity to examine the whole question of direct estimation under a more critical limelight. It is found that our knowledge of the earth's gravity field has indeed improved a great deal. However, it is not yet possible to claim definitively that our knowledge of the ocean circulation has improved through direct estimation. Yet, the improvement in the gravity model has come to the point that it is no longer possible to attribute the discrepancy at the basin scales between altimetric and hydrographic results as mostly due to geoid uncertainties. A substantial part of the difference must be due to other factors; e.g., the orbit error, or the uncertainty of the hydrographically derived dynamic topography.

1. INTRODUCTION

Since its inception, it has always been one of the most important goals of satellite altimetry to provide sea level measurements that can be readily converted to surface geostrophic currents to fix the long-standing level-of-no-motion problem once and for all (e.g., Wunsch and Gaposchkin, 1980). However, this goal has proved to be rather elusive because of large errors, which often completely overwhelm the signal. There are two major error sources, which are both related to our lack of precise knowledge of the earth's gravity field; these are the geoid uncertainty and the orbit error (i.e., uncertainty of the satellite's altitude), where the geoid is a particular equipotential surface of the earth's gravity field to which a motionless ocean would conform. The importance of the geoid stems from the simple fact that it causes the sea level to vary, relative to a reference ellipsoid (which best approximates the shape of the earth) by as much as 100 m, while the ocean dynamics can only cause variations in the range of 1 m. The orbit error is important because of its large size (of the order of 1 m). Note that the single most important contribution to the orbit error is from the imprecise gravitational force models used to derive the orbit. The geoid uncertainty is nevertheless not a problem if one is interested in the sea level variability instead. However, under no circumstances can the matter of the orbit error be avoided.

Presently, the uncertainties of independently determined geoid models are many times the amplitude of the dynamic topography. (Note that geoid models containing altimetric sea levels are much more accurate, but they cannot be used in direct estimation because they contain the dynamic topography.) As such, it seems to have precluded the possibility of direct estimation. Yet, even though the signal-to-noise ratio is unfavorable on the whole, the situation is not as bleak for the basin scales. This has been discussed at length by Tai (1983). Briefly, the large-scale features of the geoid are better known because independent geoid models are mostly products of satellite geodesy (i.e., tracking near-earth satellites to determine the earth's gravitational field; e.g., Kaula, 1966), and this procedure naturally leads to better accuracies for large scales (i.e., at the satellite altitude, it is influenced less by the small-scale features in the gravity field near the earth's surface; for example, if the satellite is far away, it can only perceive the earth as a point source). Also, geoid models and accuracy estimates are customarily given in terms of spherical harmonics because it is the natural function for expressing potential in spherical geometry (e.g., Kellogg, 1953). Reinforcing the favorable signal-to-noise ratio at the largest scales is the fact that the wavenumber spectram of the dynamic topography is rather red (Tai, 1983).

Therefore, to take advantage of the more favorable situation at the basin scales, one could subject the difference between the altimetric sea level and the geoid model to a low-pass filtering operation. One way to achieve this is to expand the difference in terms of spherical harmonics with the regions beyond data coverage (e.g., land area) set to zero and then cut off the expansion at the harmonic degree beyond which the signal-to-noise ratio becomes intolerable. This approach was taken by Tai (1983), Tai and Wunsch (1983, 84), and Englis (1985), while other forms of low-pass filtering were adopted by Douglas *et al.* (1984), Cheney *et al.* (1984). The advantage of using spherical harmonics is readily apparent; because the geoid uncertainty is the limiting factor and the uncertainty estimates are given in spherical harmonics, it is logical and desirable to analyze everything in spherical harmonics. The drawback is that oceanographers are not most familiar with spherical harmonics, not to mention the contour maps generated by the cutoff spherical harmonic expansion. The casual response is "What do the contours over land mean?" Of course, it means absolutely nothing—i.e., one would need all the high degree (small-scale) terms to make the value on land to converge to zero. Yet, the casual comment does have some ring of truth to it. The dynamic topography is meaningless over land and can be set to zero with no ill effects, but the geoid uncertainty and orbit error clearly have meaning over land. The lack of access to these useful quantities beyond data coverage causes a resolution problem (Tai, 1983), which results in spectral leakage in the sense that a large geoid uncertainty (or orbit error) contained in a particular harmonic term can spread to neighboring terms under straightforward expansion. In **Part 2** of this work, the spectral leakage problem will be remedied by least squares estimation in terms of spherical harmonics in lieu of the straightforward expansion.

The major motivation for this work is the recent release of a much more accurate independent geoid estimate GEM-T1 (Marsh *et al.*, 1987), which boasts unprecedented accuracy; e.g., the estimated uncertainty complete to degree and order 4 is only 3 cm (global rms value), which is to be contrasted with GEM-L2's 8 cm (Lerch *et al.*, 1983) and GEM-9's 16 cm (Lerch *et al.*, 1979). (Note that each degree corresponds to a wavelength approximately 40000 km divided by the degree; so degree 4 corresponds to 10000 km.) And for terms complete to degree and order 6, the estimated accuracy is within 8 cm (16 cm for GEM-L2, 30 cm for GEM-9). If these uncertainty estimates are not too optimistic, one should get considerable more mileage out of the direct estimation process. It is the intention of this work to provide a critical evaluation. We will try to mark the progress or the lack of it and identify the culprit. In **Section 2**, the methodology is reviewed with its accuracy evaluated. In

Section 3, we will try to assess at different scales the relative importance of geoid uncertainty, orbit error, and the uncertainty in the dynamic topography derived from hydrographic data. The conclusion is presented in **Section 4**.

2. METHODOLOGY

In direct estimation, we follow basically the same methods as delineated by Tai (1983) with the problem of aliasing and edge smoothing treated more rigorously. In this paper, the straight forward spherical harmonic expansion is used with altimetry-independent geoid models or with independent models supplemented by altimetry-dependent models to lessen spectral leakage. These are basically Method 1 and 3 as described by Tai (1983) and demonstrated by Tai (1983), Tai and Wunsch (1983, 1984). In **Part 2**, least squares estimation will be adopted (i.e., Method 2 and 4 in Tai, 1983).

In affixing blame (for example, what is most responsible for the discrepancy in certain scale range? Is it the geoid uncertainty or the orbit error or something else?), not only is a geoid model removed from the altimetric sea level as in the case of the direct estimation, but a dynamic topography estimate derived solely from hydrographic data (Levitus, 1982) will also be removed to create a surface composed entirely of errors (i.e., including the geoid uncertainty, orbit error, and the uncertainty of the dynamic topography estimate, e.g., due to the level of no motion assumption or due to different space time sampling).

To put these words in mathematical terms, let us define the altimetric sea level, S, to be comprised of

$$S = N + \eta + \delta r + \delta e \,, \qquad (1)$$

where N is the geoid, η is the surface dynamic topography, δr is the orbit error, and δe is the combined effect of other errors (see Tapley *et al.*, 1982; for our purpose, δe will be ignored).

Thus to estimate η directly, we remove from (1) a geoid estimate, $\hat{N}$, to get

$$D = S - \hat{N} = \eta + \delta\hat{N} + \delta r , \qquad (2)$$

where $N = \hat{N} + \delta\hat{N}$. And to further differentiate the contribution from each error source, we remove from (2) a dynamic topography estimate, $\hat{\eta}$, to get

$$F = S - \hat{N} - \hat{\eta} = \delta\hat{\eta} + \delta\hat{N} + \delta r , \qquad (3)$$

where $\eta = \hat{\eta} + \delta\hat{\eta}$. Note that there is no need to compute F and its spherical harmonic expansion, which is simply the difference between the expansions for D and $\hat{\eta}$.

Equations (1), (2), (3) are physically meaningful only at those places where the sea level has been measured by the altimeter and where a dynamic topography estimate is available. However, to do a spherical harmonic expansion, we would need values everywhere. The only sensible solution for use with the straightforward expansion is to make everything vanish outside data coverage. (In **Part 2** of this work, they are free to assume any values as long as they are outside data coverage because the least squares estimation only applies inside the data coverage.) To be specific, an overbar represents global functions that agree with the data inside data coverage but vanish outside. When a global function with an overbar is expanded, it presents a spectral leakage problem for $\delta\hat{N}$ and δr (see Section 2.2 in Tai, 1983), while this is basically not a problem for $\hat{\eta}$ and $\delta\hat{\eta}$ because both are undefined over land. As such, one must realize—when comparing the degree variances of an estimate of the geoid uncertainty, $\delta\hat{N}$, with its counterpart derived from (3), $\overline{\delta\hat{N}}$ —that he is comparing related but different quantities. (Note that the degree variances in spherical harmonic expansion correspond to the wavenumber spectrum in Fourier analysis.)

The straightforward spherical harmonic expansion in practice presents two problems, i.e., the aliasing problem and the edge-smoothing (a.k.a., data window tapering) problem. These will be explored in some detail. In previous works, running average after the mean had been removed (20° by 20° for Tai, 1983; Tai and Wunsch,

1983; 10° by 10° for Tai and Wunsch, 1984) were conducted (in association with an expansion complete to harmonic degree and order 36) to remove the high degree energy (therefore lessen aliasing) and smooth the edges of data boundaries. A 10° by 10° average removes most of the terms of degrees higher than degree 36, but it also reduces the energy close to degree 36. This was adequate for previous works because the geoid model used then was GEM-9, which was only complete to degree and order 20. (The running average was perhaps the preferred procedure because the spectral leakage was much more serious for a less accurate and complete geoid model.) Now GEM-T1 is complete to degree and order 36 and its accuracy is to be assessed independently here; we clearly would need a new procedure. First, the spherical harmonic expansion is extended to degree and order 90 to reduce the potential for aliasing. The expansion procedure is still based on the fast Fourier transform (Goldstein, 1978; also see Tai, 1983). This algorithm has been optimized for the San Diego Supercomputer Center's Cray XMP-48 so that it takes only 0.18 seconds CPU time to expand a global data on 2° by 2° grid. Second, instead of running averages extended beyond data coverage to smooth the data boundary, a sine data window is adopted to smooth the transition to zeroes outside data coverage, i.e., the data window has the form

$$w = \begin{cases} 1 & \text{, if the nearest boundary is at least } 7^\circ \text{ away} \\ \sin\left(\frac{\theta}{7}\,\frac{\pi}{2}\right) & \text{, if the nearest boundary is } \theta \text{ degree away} \end{cases} \tag{4}$$

(a) Strategy

Our aim is to produce the direct estimation and assess the relative importance of error sources. To achieve this, three geoid models (GEM-T1; GEM-L2; PGS-S4, see Lerch *et al.*, 1982) and their combinations are used. (Note that GEM-T1 and GEM-L2 are derived solely from satellite tracking, while PGS-S4 also includes altimeter data as additional tracking. Hence, GEM-T1 and GEM-L2 are independent estimates of the geoid, but PGS-S4 is correlated to some extent with the dynamic topography.) A well-balanced strategy would require that one try a variety of orbits computed from different earth's gravitational models and tracking data as well, and one use different dynamic topography estimates computed from different hydrographic data of various data durations and extents with different assumptions and methods. However, these are not readily available. Thus, the SEASAT

altimetric sea level (Rapp, 1983) and Levitus' (1982) dynamic topography (0-2250 db), which were both used in previous studies, are still the only ones used in this study. We hope to remedy the sitluation shortly. Subscripts (indices) are appended to distinguish results computed from different geoid models or different methods. These are explained in Table 1.

(b) Aliasing

To reduce aliasing, 5° by 5° running average with no extension beyond data coverage is conducted. The results (with subscript u) can be compared with those (with subscript a) without averaging. Square roots of degree variances for $\overline{D}$, $\overline{F}$, and $\overline{\hat{\eta}}$ are tabulated in Table 2, 3, and 4. Substantial aliasing can result for $\overline{D}$ and $\overline{F}$, especially in degree band 21 to 36 (while disastrous for degree 37-90), but somewhat insignificant in degree 1 through 8. The situation is different for $\overline{\hat{\eta}}$. There is insignificant aliasing because there is little energy in Levitus' surface (a century-long average) beyond degree 90 (about 400 km).

(c) Edge Smoothing

Edge smoothing (or tapering) serves two related purposes. It reduces the sharp changes at data boundaries where Gibbs phenomenon can result. And it also reduces side lobes, which in turn reduces spectral leakage (i.e., increasing resolution). The effects of edge smoothing are clearly significant especially for high degree terms when one compares terms with the subscript u (edge unsmoothed) with those with the subscript 1. However, one should note that the data coverage (i.e., where SEASAT altimetric sea level and Levitus' dynamic height, 0-2250 db, are both available) constitutes 58.12% of the earth's surface, and the sine window effectively reduces it to 47.95%.

(d) Pattern Correlation

It will soon become obvious that $\overline{D}$ and $\overline{\hat{\eta}}$ are significantly different in amplitude (i.e., $\overline{F}$ is large), but they are quite similar in shape for the first few degrees. Thus to quantify the resemblance, let us define the pattern correlation in degree band L_1 to L_2 as

$$\frac{\sum_{l=L_1}^{L_2}\sum_{m=-l}^{l}\overline{D}_l^m\,(\overline{H}_l^m)^*}{\left(\sum_{l=L_1}^{L_2}\sum_{m=-l}^{l}|\overline{D}_l^m|^2\right)^{1/2}\left(\sum_{l=L_1}^{L_2}\sum_{m=-l}^{l}|\overline{H}_l^m|^2\right)^{1/2}}\ , \qquad (5)$$

where $\overline{D}_l^m$ and $\overline{H}_l^m$ are the complex spherical harmonic coefficients of $\overline{D}$ and $\overline{\hat{\eta}}$, and ( )* means complex conjugate.

3. RESULTS

The discussion is classified into four catefgories: (a) direct estimation; (b) geoid uncertainty; (c) orbit error; (d) uncertainty of the hydrographically derived dynamic topography.

(a) Direct Estimation

For now, the geoid uncertainty is still the limiting factor. To see its effect, the uncertainty estimates of GEM-T1, the differences of GEM-L2, PGS-S4, and GEM-T1 with one another are listed in Table 5. However, extra care must be taken when comparing these terms directly with terms in Table 2, 3, and 4. The resolution (spectral leakage) problem can be thought of as smearing individual terms to produce an averaged result (i.e., high uncertainty and high accuracy are both somewhat reduced). Also, the data window effectively reduces the power to 47.95% level. To account for this effect, each term in Table 5 is multiplied by 0.4795 and tabulated alongside the original term. Comparing $\overline{\hat{\eta}}$ with $\delta\hat{N}_1$ x 0.4795, it is apparent that the noise exceeds the signal at degree 9 and beyond. This is further confirmed by the pattern correlation analysis, which is tabulated in Table 6. The pattern correlation suffers a dip (or even becomes negative) at degree 9. Hence, direct estimates will be presented only complete to degree 8 or lower.

To determine which geoid model yields the best results, two criteria are used, i.e., the pattern correlation (the higher the better), and the discrepancy $\overline{F}$ (the lower the better). In terms of pattern correlation (see Table 6) between degree 1 through 6, the best result is provided by $\hat{N}_8$ (i.e., a hybrid with terms of degree 2 through 8

from GEM-T1 and terms of degree 9 through 36 from PGS-S4), followed by $\hat{N}_6$ (GEM-T1 degree 2-6 and PGS-S4 degree 7-36), $\hat{N}_1$ (GEM-T1) and $\hat{N}_3$ (GEM-L2 degree 2-6 and PGS-S4 degree 7-36), $\hat{N}_4$ (PGS-S4), and $\hat{N}_2$ (GEM-L2). The order remains the same except for a switch in position of $\hat{N}_1$ and $\hat{N}_6$ when the pattern correlation complete to degree 8 is considered. In terms of the discrepancy (see **Table 3**) complete to degree 6, $\hat{N}_8$ again turns in the best performance, to be followed by $\hat{N}_6$ (a very close second), $\hat{N}_1$, $\hat{N}_4$, $\hat{N}_3$, and $\hat{N}_2$. When the discrepancy up to degree 8 is considered, $\hat{N}_6$ jumps in front of $\hat{N}_8$ by a small margin. The performance can be clearly differentiated into two levels. In the lower end, $\hat{N}_2$ (GEM-L2) is by far the worst performer, followed by $\hat{N}_4$ (PGS-S4) and their hybrid $\hat{N}_3$ (note the pattern correlation is rather good for $\hat{N}_3$). On the other end, $\hat{N}_8$ is arguably the best, although the discrepancy increases in degree 7 and 8 for $\hat{N}_8$ versus $\hat{N}_6$ (see Table 3). Nevertheless, the increase could be attributed to the fact that PGS-S4 contains contributions from the dynamic topography. Otherwise, how else can it be explained that for $\hat{N}_1$ (GEM-T1) the pattern correlation actually improves when the expansion is extended to degree 8 from degree 6? Thus, one can tentatively conclude that currently the best geoid estimates are provided by GEM-T1 through degree 8, but for degree 9 and beyond, PGS-S4 is better than GEM-T1. Hence, $\hat{N}_8$, which uses the best geoid estimates provided by GEM-T1 through degree 8, and reduces the spectral leakage stemming from geoid uncertainties of degrees 9 and higher, is the best choice for direct estimation up to spherical harmonic degree 8.

$\overline{D}_8$ (direct estimate), $\overline{F}_8$ (discrepancy), and $\overline{\hat{\eta}}$ (Levitus' dynamic topography, 0-2250 db) complete to degree 6 are displayed in Fig. 1, up to degree 8 in Fig. 2. In all the contour maps, the zero contour is thickened and represented by chain dashed lines, while the positive (negative) contours are repesented by solid (dashed) lines with every third contour from zero thickened and labeled (in meters). It is evident that there is strong visual correlation between $\overline{D}_8$ and $\overline{\hat{\eta}}$ as manifested by the high correlation numbers in Table 6. It is also clear that the amplitude of $\overline{D}_8$ is about twice that of $\overline{\hat{\eta}}$ and there are major disagreements in shape as well, most notably in the Indian Ocean. On the positive side, all major gyres including the Circumpolar Current and even the subarctic gyres are in the right direction (except the Indian Ocean). The good agreement in the Circumpolar Current region is not only in shape but also in amplitude. This is borne out by the discrepancy maps showng smooth difference generally less than 20 cm in the region. The altimetric results, in contrast to the hydrographic results, show a second high in the South Pacific next to South America, which is not all that unbelievable because observed

surface current patterns do show a similar feature (Meehl, 1982). On the negative side, the pattern is completely amiss in the Indian Ocean. The discrepancy maps, which contain contributions from all error sources, either show that all the geoid models underestimate the geoid low in the Indian Ocean. (Note that the circulation pattern is wrong here for all models. The GEM-T1 complete to degree 8 is shown in Fig. 3), or the orbit error causes this low—more discussions on this in **Subsection (c)**. The altimetric results have twice the amplitude. Can the true dynamic topography during the period July to September 1978 have twice the amplitude than that of Levitus' result? The discussion is postponed until **Subsection (d)**.

(b) Geoid Uncertainties

In this section, the geoid models will be assessed in three degree bands, and how much of the discrepancy complete to degree 8 can be attributed to geoid uncertainties will also be discussed. Starting with the easier part, one can safely assume that the discrepancies in degree bands 9-20 and 21-36 are dominated by geoid uncertainties. For degree band 9-20 in Table 3, GEM-L2 ($\overline{F}_2$) has the largest discrepancy, and GEM-T1 ($\overline{F}_1$), cut that in half, while PGS-S4 cut it in half again. For degree band 21-36, GEM-L2 is only complete to degree 20 with a few additional terms. Thus, $\overline{F}_2$ almost represents the energy content of the marine geoid in this degree band. GEM-T1 does a reasonable job in cutting it from 65 cm to 47 cm, which is further reduced to 26 cm by PGS-S4. It is reasonable to conclude that in degree band 9-36, tremendous strides have been made in improving the independent geoid estimates; however, they still have a long way to go before they can match the accuracy of geoid models containing altimetry. Efforts to improve the geoid model (like the one yielding GEM-T1) undoubtedly will soon produce better products than GEM-T1. However, it is the author's belief that the ultimate solution to the geoid problem can only come from satellite to satellite tracking such as the proposed Geopotential Research Mission (Taylor *et al.*, 1982). In the meantime, it is all right to use the dependent geoid models to compute the orbit.

The situation in degree band 0-8 is somewhat different. Judging from the evidence provided by the pattern correlation and the discrepancy, GEM-T1 is better than PGS-S4. The fact that PGS-S4 is correlated with the dynamic topography, but still yields a bigger discrepancy than GEM-T1 does not bode well for dependent geoid models as the suitable geoid model in direct estimation. As a matter of fact, although $\hat{N}_3$ yields a slightly larger

discrepancy than PGS-S4 (which is to be expected given PGS-S4's correlation with the dynamic topography), it has clearly better pattern correlation; i.e., even GEM-L2 up to degree 6 is better than PGS-S4 in the corresponding range if the spectral leakage from degree 7 and beyond can be lessened.

Now comes the tough question of how much of the discrepancy in degree 0-8 is due to geoid uncertainties. According to Marsh *et al.* (1987), the uncertainty of GEM-T1 up to degree 6 is only 7.57 cm (effectively 3.63 cm, ignoring spectral leakage), and 14.53 cm (effectively 6.97 cm) if up to degree 8. If these error estimates are realistic, than geoid uncertainties are really minor factors. The question is: are they realistic? One can check the internal consistency of these error claims using **Table 3** and **5** with the help of the following formulas:

$$N = \hat{N}_1 + \delta\hat{N}_1 = \hat{N}_2 + \delta\hat{N}_2 = \hat{N}_4 + \delta\hat{N}_4,$$

and

$$\hat{N}_2 - \hat{N}_1 = \delta\hat{N}_1 - \delta\hat{N}_2,$$

$$\hat{N}_4 - \hat{N}_1 = \delta\hat{N}_1 - \delta\hat{N}_4.$$

For example, $\delta\hat{N}_2$ is 8 cm complete to degree 4, 16 cm to degree 6, while $\delta\hat{N}_1$ up to degree 4 is 2.91 cm. Thus the range of $\hat{N}_2 - \hat{N}_1$ up to degree 4, according to the uncertainty estimates, is 5.09 cm to 10.91 cm. If $\delta\hat{N}_1$ and $\delta\hat{N}_2$ are assumed to be independent, one would come up with a number of 8.51 cm. The actual difference, up to degree 4, is 9.33 cm. Complete to degree 6, the range is 8.43 cm to 23.57 cm, 17.7 cm if independent, and the actual number is 19.91 cm. Thus, $\delta\hat{N}_1$ and $\delta\hat{N}_2$ tend to be negatively correlated, while one would expect them to be positively correlated because a substantial part of the satellite tracking used to derive these two models is shared. For the purpose of consistency check, one could use $\overline{F}_4$ in place of $\delta\hat{N}_4$ in degree 9-36. One would find $\delta\hat{N}_1$, and $\delta\hat{N}_4$, to be substantially, negatively correlated in degree 9-20 (actually a difference of 59.79 cm versus 47.69 cm if independent), much less so for degree 21-36 (69.24 cm versus 67.57 cm), when one would expect them to be independent. Direct comparison of $\overline{F}_1$ and $\delta\hat{N}_1$ leads to the conclusion that uncertainty estimates are too optimisitc in degree 9-20, while too pessimistic in degree 21-36. Direct comparison of each

degree (not shown here) confirms that the uncertainty claim tends to underestimate the discrepancy for degree 16 and less, and overestimate for degree 17 and higher. So it is reasonable to conclude that the uncertainty estimates are too optimistic for the low degrees. However, only after a five-fold increase in the uncertainty estimates (ignoring spectral leakage) can one even start to account for just half of the discrepancy in degree 0-6. A substantial part of the difference must be attributed to other factors. The spectral leakage from higher degree more uncertain geoid terms is not believed to be a major factor because the result based on GEM-L2 alone (i.e., $\hat{N}_2$) do not differ signficiantly in pattern from other results, yet it suffers significant spectral leakage (comparing to the result based on $\hat{N}_3$). Nonetheless, the spectral leakage problem will be taken care of in **Part 2** of this work, using a least squares estimation procedure in terms of spherical harmonics. Faced with the wrong circulation pattern in the Indian Ocean, the only remaining recourse is to blame it on the orbit error.

(c) Orbit Error

The orbit released with the SEASAT data has an accuracy of 1.2 m, which is most evident at the crossover point of two satellite ground tracks, where the orbit error causes the two altimetric sea level readings to differ by over 1.5 m on average (called the crossover difference). Clearly, one would not have been able to deduce any meaningful circulation patterns if this had not been reduced. A practical and effective way to achieve this has been devised and dubbed the crossover adjustment method, which can be explained briefly as follows. Along track, the orbit error is a very large-scale feature with a dominant spectral peak at once per revolution (about 40,000 km in wavelength; e.g., Cutting *et al.*, 1978; Marsh and Williamson, 1980). The satellite track is interrupted by land and data gaps into segments, most of which are typically a small fraction in length in comparison to one revolution; and the orbit error appears as a bias and a tilt (i.e., mean and trend) along most of the segments. If each segment is assigned two unknowns representing the bias and tilt, then one can solve for the orbit error represented by those biases and tiles that account for the observed crossover differences in the least squares sense.

Rapp's surface (which is being used in this study) was adjusted for the bias and tilt to reduce the rms crossover difference from 1.5 m to 28 cm. However, in a global adjustment, there are many long segments for which the linear representation is inadequate. For example, one commit 9% rms relative error in representing a sine wave by a straight line over a quarter wavelength (9% of 1.2 m is 11 cm), 19% for three-eighth of a

wavelength (19% of 1.2 m is 23 cm), 32% for half a wavelength (see Tai, 1988a). Furthermore, in crossover adjustments, it is necessary to fix one or more segments (or apply other constraints) to remove the arbitrariness inherent in the solution; for example, a constant (but otherwise arbitrary) bias can be added to all segments without affecting the crossover differences. In Rapp's surface, a well-tracked long segment in the Atlantic Ocean is fixed, i.e., the orbit error along this segment remains. By fixing a different segment located in the Pacific Ocean, the resulted difference has a mean of 15 cm with a standard deviation of 7 cm. Because of the long wavelength nature of the orbit error, one would expect the error stemming from the fixed track to be concentrated in the first few harmonic degrees. In addition, there is the geographically dependent orbit eror, which does not manifest itself in the crossover difference, therefore cannot be removed by the crossover adjustment. If the spectrum of the orbit error is really as concentrated near the once per revolution as the orbit error simulations have shown, then the geographically dependent orbit error is also contained in the first few harmonic degrees, mainly degree one corresponding to the once per revolution peak (Tai and Fu, 1986).

To further differentiate the information contained in each degree, maps for each degree alone (for the best results based on $\hat{N}_8$) are displayed in Fig. 4 (for degree 1), Fig. 5 (degree 2), Fig. 6 (degree 3), and Fig. 7 (degree 6). These degrees are selected because they are the most energetic components and degree 2 and 3 (to a lesser extent, the degree 1 terms as well) are most responsible for the wrong circulation pattern in the Indian Ocean. The relevant results based on $\hat{N}_8$ are collected from the other tables to form Table 7 to facilitate one-stop comparison. For degree 1, it is amazing to see in Fig. 4 how $\overline{D}_8$ and $\overline{\hat{\eta}}_8$ resemble each other (the pattern for $\overline{D}_8$ is shifted a little to the east). The visual impression is reinforced in Table 7 by the high correlation and the fact that the energy level of $\overline{F}_8$ at degree 1 is almost a straight cancellation from those of $\overline{D}_8$ and $\overline{\hat{\eta}}$ (note that a perfect match in shape but difference in amplitude would give a number 16 cm versus 17.72 cm in Table 7). There is no degree 1 components in the geoid (Heiskanen and Moritz, 1967). Hence (save for the spectral leakage effect) the difference at degree 1 is due to either the orbit error or real difference in the dynamic topography. If the difference is all due to the orbit error, it is indeed quite unusual to find the orbit error to be so highly correlated with $\overline{\hat{\eta}}$. But, whatever portion of the degree 1 discrepancy is due to the orbit error, it may indeed have contributed to the wrong circulation pattern in the Indian Ocean because the discrepancy shows a low to the east of South Africa (in the Indian Ocean) instead of to its southwest (in the South Atlantic) as shown in the map for $\overline{\hat{\eta}}$. The discrepancy

map for degree 2 in Fig. 5 has a big contribution toward the wrong circulation pattern in the Indian Ocean, while its counterpart for degree 3 in Fig. 6 shows a slightly smaller contribution. But overall, $\overline{D}_g$ and $\overline{\hat{\eta}}$ are much better correlated at degree 2 than at degree 3. The reason may well be that the dynamic topography is much more energetic at degree 2 than at degree 3 (degree 2 is the most energetic part according to $\overline{\hat{\eta}}$), and thus can tolerate more orbit error before being overwhelmed. In Fig. 7, the degree 6 maps demonstrate a strong visual corelation between $\overline{D}_g$ and $\overline{\hat{\eta}}$ except for the fact that the amplitudes have about a 3 to 2 ratio (note all contour intervals in Fig. 7 are 5 cm).

Now there is little doubt that the wrong circulation pattern is caused by the orbit error in Rapp's surface. This argument is strengthened by the investigations presented by Cheney *et al.* (1984, see their Fig. 7) and Douglas *et al.* (1984, see their Fig. 3), which show better correlation with $\overline{\hat{\eta}}$ in the Indian Ocean because they have used different surfaces and have treated the orbit error differently. This would in no way diminish the value of Rapp's surface, which is considered one of the best (if not the best available). One may go one step further to assert that the geographically dependent error is not the main cause (because if it is, all three investigations should have this common problem). However, it is hard to resist pointing out the similarity between Fig. 2C and Fig. 3, or between Fig. 3 and Fig. 5C with the implication that if the geoid model should underestimate the highs and lows, a similarly shaped geographically correlated orbit error would result (Tapley and Rosborough, 1985, see their Fig. 7 and 9).

Recently, Tai (1988b) has put forth a new crossover adjustment technique, which uses a sine wave to represent the orbit error in each revolution, and minimizes not only the crossover differences but the orbit adjustment as well so that there is no need to fix any segments in the adjustment. The new technique is simpler (no need to remember which segments have been fixed; no need to assign different numbers of unknowns according to the length of each segment—it is the usual practice to assign a bias for short segments, a bias and tilt for long segments, even add a curvature term for extra-long segments, i.e., to use as many unknowns as warranted to keep the problem size manageable), more accurate (see Tai, 1988a) and consistent (i.e., separate segments but consecutive in time will be assigned consistent orbit errors)—and much more efficient because the number of unknowns is much less (one revolution is usually separated into 5 to 8 segments). The SEASAT data can be readjusted or the new GEOSAT data can be adjusted to provide more realizations of the residual orbit error.

Furthermore, accompanying the development of more accurate geoid models, there has been a series of more accurate SEASAT orbits with the latest one claiming accuracy of 0.42 m (Marsh *et al.*, 1987) to be contrasted with the unadjusted orbit error of 1.2 m in the original SEASAT data. As mentioned in **Section 2**, a well-balanced strategy would demand that more realizations be obtained on orbit errors to gain better understanding.

(d) Uncertainty in the Hydrographically Determined Dynamic Topography

Two areas can be identified almost immediately as potential sources for legitimate differences between the altimetric and hydrographic results. First is the level of no motion problem. Levitus' surface only represents the relative dynamic topography (surfaces versus 2250 db). Uncertainties of 10 cm (rms) in the open sea, and 25 cm in the vicinity of the Gulf Stream have been suggested for the North Atlantic dynamic topography determined by the inverse method (Wunsch, 1981; Roemmich and Wunsch, 1982), which makes the circulation (implied by the hydrographic data) conserve mass and conservative tracers. Thus, over 30 cm difference as shown in **Table 7** is way too big. There is another way to establish an upper limit on the effect of flows at the reference level. Assuming mid-latitude conditions (i.e., $f = 10^{-4}$ sec.) and an average ocean depth of 4000 m, one can estimate the additional transport resulted from motions at the level of no motion. And, it translates to a number of about 4-sverdrup additional transport for each additional centimeter of elevation difference across a section. Thus, a 10-cm difference would mean a 40-sverdrup difference in transport (this number depends critically on the depth). Clearly, one should not expect the level of no motion assumption to cause a difference of cross-basin slope, much more than 10 cm.

The second area where real differences can arise is in what can be termed "the 3 months versus history problem." Levitus' surface contains all the available hydrographic data, whereas the SEASAT surface is only a three-month average for the period July to September 1978. Basin-scale circulations do exhibit considerably variability, both annually and interannually (a dramatic example is furnished by Fofonoff and Tabata, 1966, for the Alaskan Gyre). This has been discussed at length in Tai (1983, please refer to the many references cited there); briefly, annual changes like 12 dyn-cm in the west and 7 dyn-cm in the east have been observed for the North Pacific, and considerable seasonal variations can occur in its components (e.g., the Kuroshio, the North Equatorial Current, etc.), and finally, the maximum range of interannual variability about the long-term mean can be as high

as 25%. The highest slope in $\overline{\hat{\eta}}$ complete to degree 8 is 70 cm across the North Pacific; 25% of it gives 17.5 cm. How the ocean responds to various forcings is an extremely interesting, albeit difficult problem (a concise but penetrating discussion can be found in Charney and Flierl, 1981). The spin-up time (baroclinic response) of the ocean to wind forcing is measured in years in the mid-latitude, while it can respond within months in the tropics. However, slow response does not mean no response, but a delayed response does tend to smooth-out the sharp changes in the forcing. The ocean can respond barotropically within days, yet, as discussed in the previous paragraph, the response is not expected to exceed a few centimeters in terms of the sea level.

4. CONCLUSION

It is found that the geoid model has improved to the point that it is no longer the biggest source of error in the direct estimation of basin-scale ocean circulations. Instead, the orbit error has become the culprit. Although not used in this study, the orbit error has also been reduced. A follow-up study should use the best orbit available. In order to make a real contribution to the basin-scale circulation problem, the combined accuracy of satellite altimetry in the largest scales must go below 10 cm. There is every indication that this goal is attainable for the upcoming TOPEX/POSEIDON mission (Steward, *et al.*, 1986).

ACKNOWLEDGMENTS

J. Marsh made the geoid model GEM-T1 available for this analysis. Programming support by Paul Rasmussen is acknowledged. Support by NASA Grant NAGW 808. The computation was done on the San Diego Supercomputer Center's CRAY XMP-48.

REFERENCES

Charney, J.G. and G.R. Flierl, 1981: Oceanic analogues of large-scale atmospheric motions. In: *Evolution of Physical Oceanography*, B.A. Warren and C. Wunsch, eds., MIT Press, Cambridge, Mass. 623 pp.

Cheney, R.E., B.C. Douglas, D.T. Sandwell, J.G. Marsh, T.V. Martin, and J.J. McCarthy, 1984: Applications of satellite altimetry to oceanography and geophysics. *Marine Geophys. Res.*, **7**, 17-32.

Cutting, E., G.H. Born, and J.C. Frautnick, 1978: Orbital analysis for SEASAT-A. *J. Astronaut Sci.*, **26**, 315-342.

Douglas, B.C., R.W. Agreen, and D.T. Sandwell, 1984: Observing global ocean circulation with SEASAT altimeter data. *Mar. Geod.*, **8**, 67-83.

Englis, T., 1985: Global circulation from SEASAT altimeter data. *Mar. Geod.*, **9**, 45-69.

Fofonoff, N.P. and S. Tabata, 1966: Variability of oceanographic conditions bestween ocean stations P and Swiftsure Bank of the Pacific Coast of Canada. *J. Bul. Res. Brd. Canada*, **23**, 825-868.

Goldstein, J.D., 1978: Application of Fourier techniques to the computation of spherical harmonic coefficients. *Tech. Information Memo.* The Anal. Sci. Corp., Reading, Mass.

Heiskanen, W.A. and H. Moritz, 1967: *Physical Geodesy.* W.H. Freeman, San Francisco, Calif., 364 pp.

Kaula, W.M., 1966: *Theory of Satellite Geodesy.* Blaisdell, Waltham, Mass., 124 pp.

Kellogg, O.D., 1953: *Foundations of Potential Theory.* Dover, New York, New York.

Lerch, F.J., S.M. Klosko, R.E. Lambscher, and C.A. Wagner, 1979: Gravity model improvement using GEOS 3 (GEM 9 and 10). *J. Geophys. Res.*, **84**, 3897-3916.

———————— , ———————— , and G.B. Patel, 1982: A refined gravity model from LAGEOS (GEM-L2). *Geophys. Res. Lett.*, **9**, 1263-1266.

———————— , J.G. Marsh, S.M. Klosko, and R.G. Williamson, 1982: Gravity model improvement for SEASAT. *J. Geophys. Res.*, **87**, 3281-3296.

Levitus, S., 1982: Climatological Atlas of the World Ocean, NOAA Prof. Pap., 13, U.S. Dept. of Commerce, 173 pp.

Marsh, J.G. and R.G. Williamson, 1980: Precision orbit analyses in support of the SEASAT altimeter experiment. *J. Astronaut. Sci.*, **28**, 345-369.

———————— , and seventeen other collaborators, 1987: An improved model of the earth's gravitational field: GEM-T1. *NASA Tech. Memo, 4019.* Goddard Space Flight Center, Greenbelt, MD.

Meehl, G.A., 1982: Characteristics of surface current flow inferred from a global ocean current data set. *J. Phys. Oceanogr.*, **12**, 538-555.

Roemmich, D. and C. Wunsch, 1982: On combining satellite altimetry with hydrographic data. *J. Mar. Res.*, **10**, 605-619.

Stewart, R., L.-L. Fu, and M. Lefebvre, 1986: Science opportunities from the TOPEX/POSEIDON mission. *JPL Publication 86-18.* NASA-Jet Propul. Lab., Pasadena, Calif.

Tai, C.-K., 1983: On determining the large-scale ocean circulation from satellite altimetry. *J. Geophys. Res.*, **88**, 9553-9565.

————— , 1988a: Error assessments of widely-used orbit error approximations in satellite altimetry. *J. Atmos. Oceanic Tech.*, in press.

————— , 1988b: Geosat crossover analysis iln the tropical Pacific. Part 1. Constrained sinusoidal crossover adjustment. *J. Geophys. Res.*, in press.

————— , and C. Wunsch, 1983: Absolute measurement of the dynamite topography of the Pacific Ocsean by satellite altimetry. *Nature*, **301**, 408-410.

————— , and ————— , 1984: An estimate of global absolute dynamic topography. *J. Phys. Oceanogr.*, **14**, 457-463.

————— , and L.-L. Fu, 1986: On crossover adjustment in satellite altimeltry and its oceanographic imlplications. *J. Geophys. Res.* **91**, 2549-2554.

Tapley, B.D., G.H. Born, and M.E. Parke, 1982: The SEASAT altimeter data and its accuracy assessment. *J. Geophys. Res.*, **87**, 3179-3188.

Tapley, B.D. and G.W. Rosborough, 1985: Geographically correlated orbit error and its effect on satellite altimetry mission. *J. Geophys. Res.*, 90,. 11817-11831.

Taylor, P.T., T. Keating, W. D. Kahn, R.A. Langel, D.E. Smith, and Schnetzler, 1983: GRM: observing the terrestrial gravity and magnetic fields in the 1980's. *EOS Trans. AGU*, **64**, 609-611.

Wunsch, C., 1981: An interim relative sea surface for the North Atlantic Ocean. *Mar. Geod.*, **5**, 103-119.

Wunsch, C. and E.M. Gaposchkin, 1980: On using satellite altimetry to determine the general circulation of the ocean with appication to geoid improvements. *Rev. Geophys. Space Phys.*, **18**, 725-745.

FIGURE LEGENDS

Fig. 1. Spherical harmonic expansion complete to degree and order 6 for (a) $\overline{D}_8$, (b) $\overline{\hat{\eta}}$, and (c) $\overline{F_8}$.

Fig. 2. Same as Fig. 1 except complete to degree and order 8.

Fig. 3. GEM-T1 complete to degree and order 8.

Fig. 4. Degree 1 results for (a) $\overline{D_8}$, (b) $\overline{\hat{\eta}}$, and (c) $\overline{F}_8$.

Fig. 5. Same as Fig. 4 except for degree 2.

Fig. 6. Same as Fig. 4 except for degree 3.

Fig. 7. Same as Fig. 4 except for degree 6.

(a)

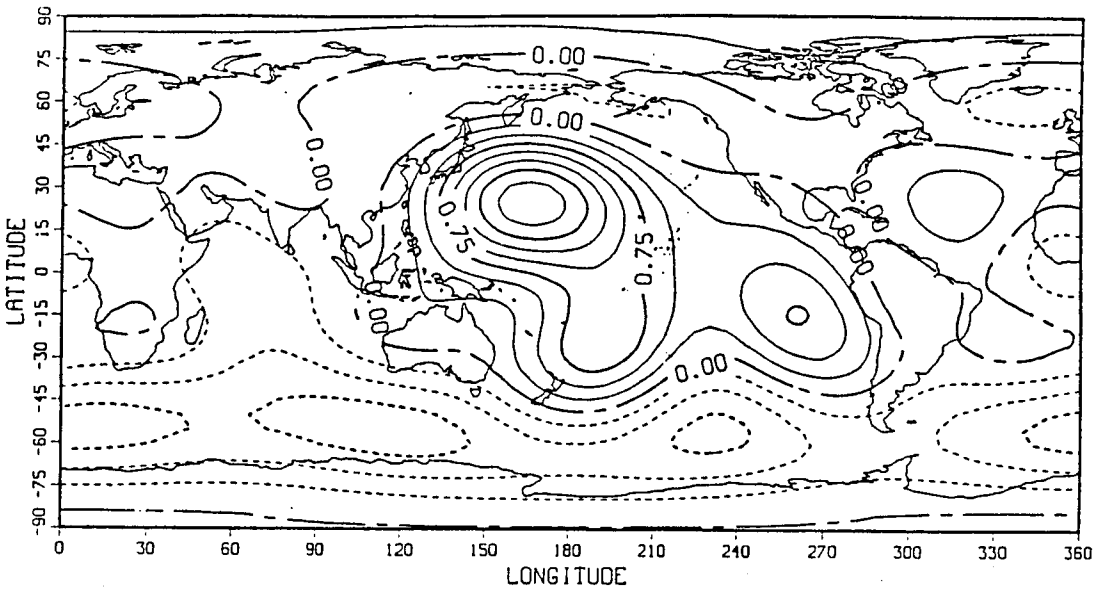

(b)

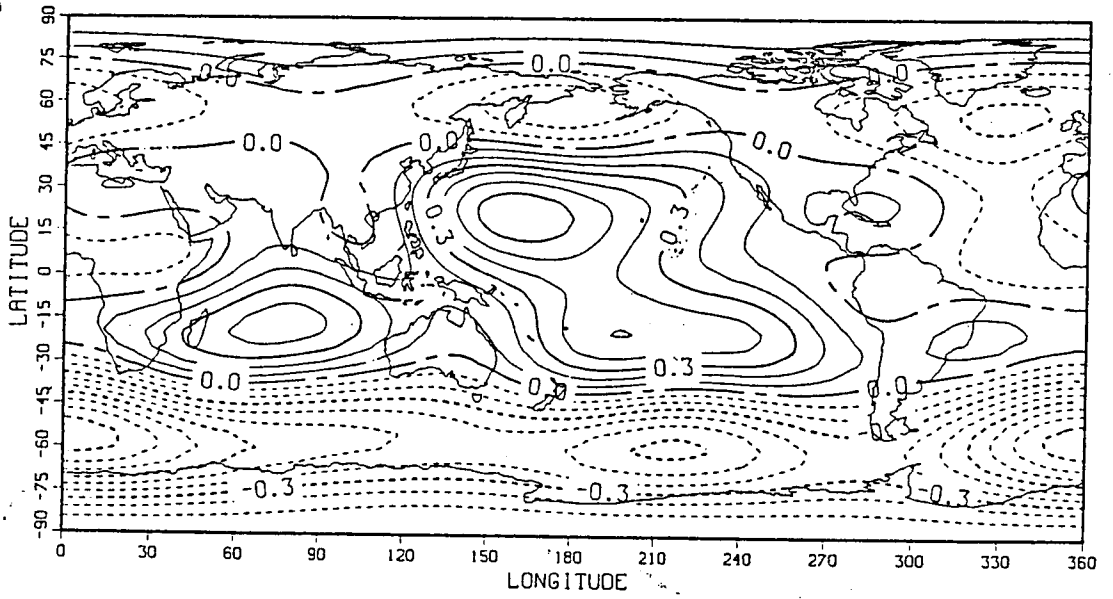

(c)

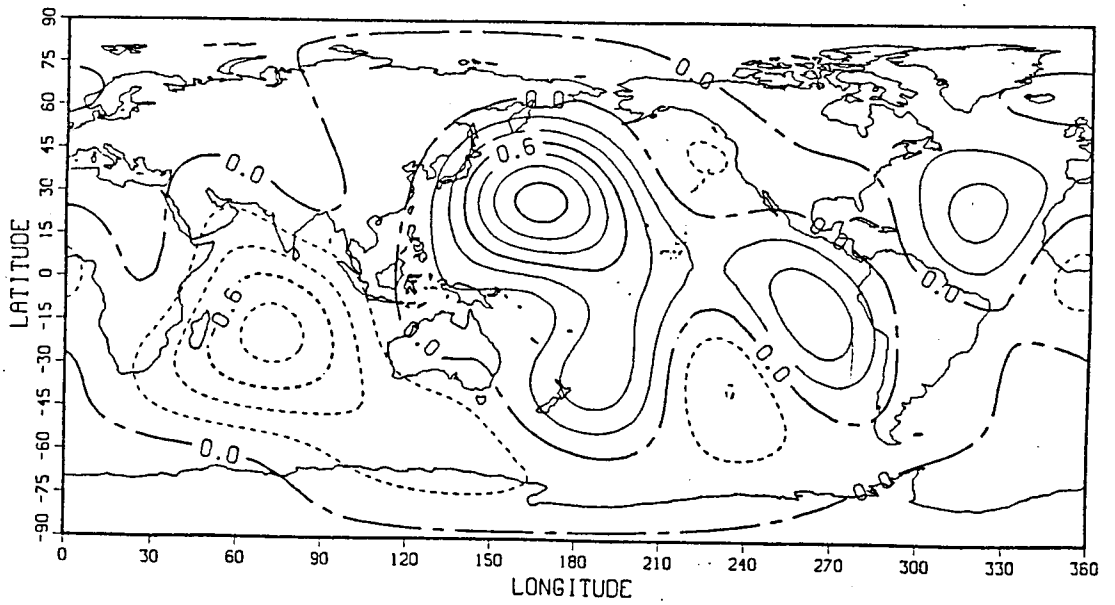

Fig. 1

(a)

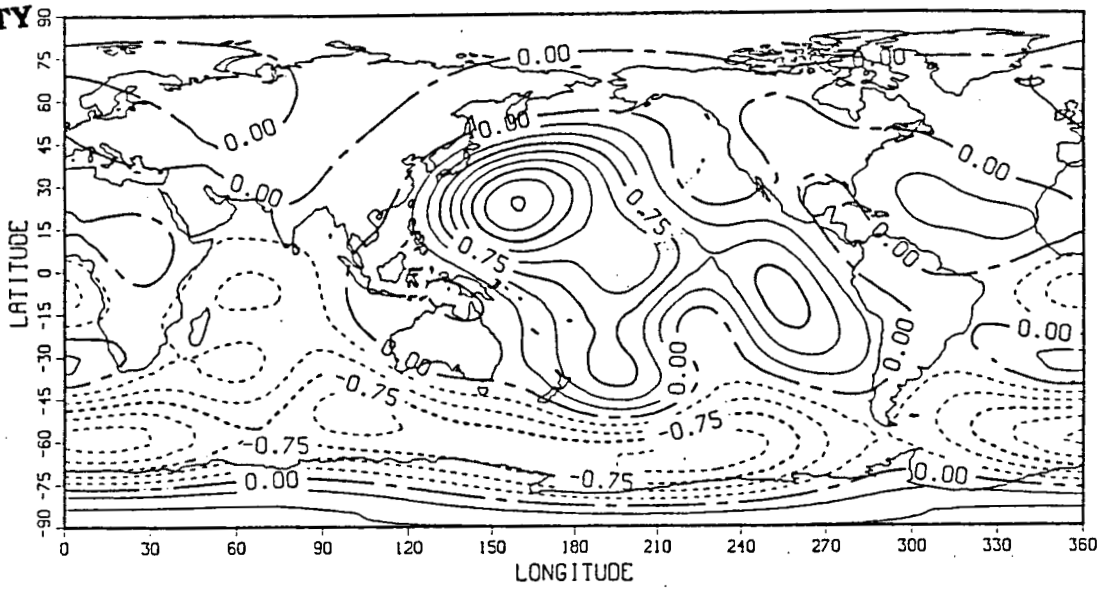

(b)

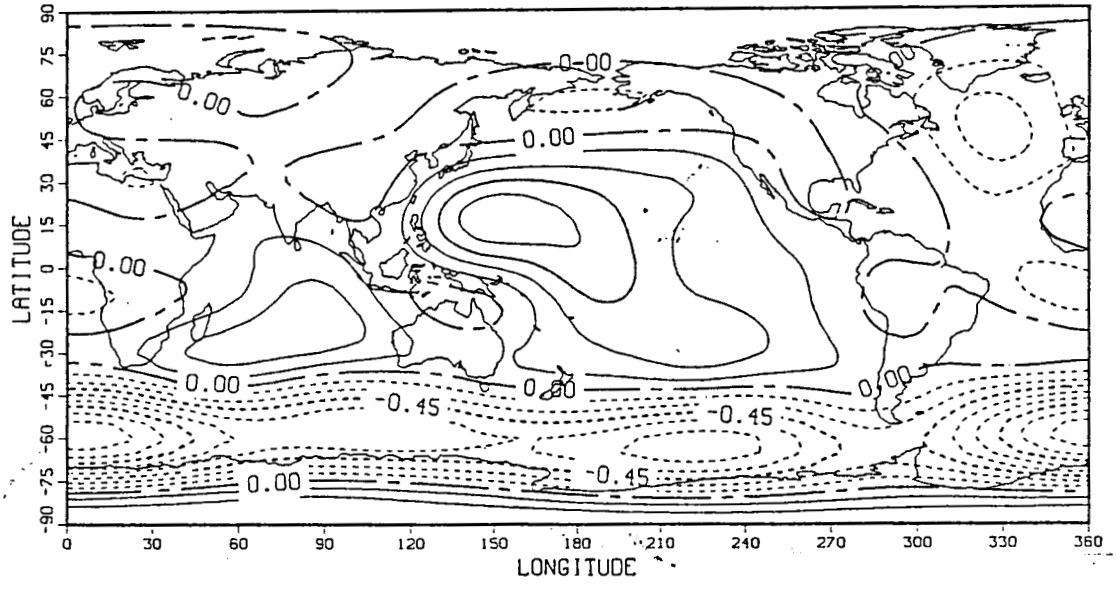

(c)

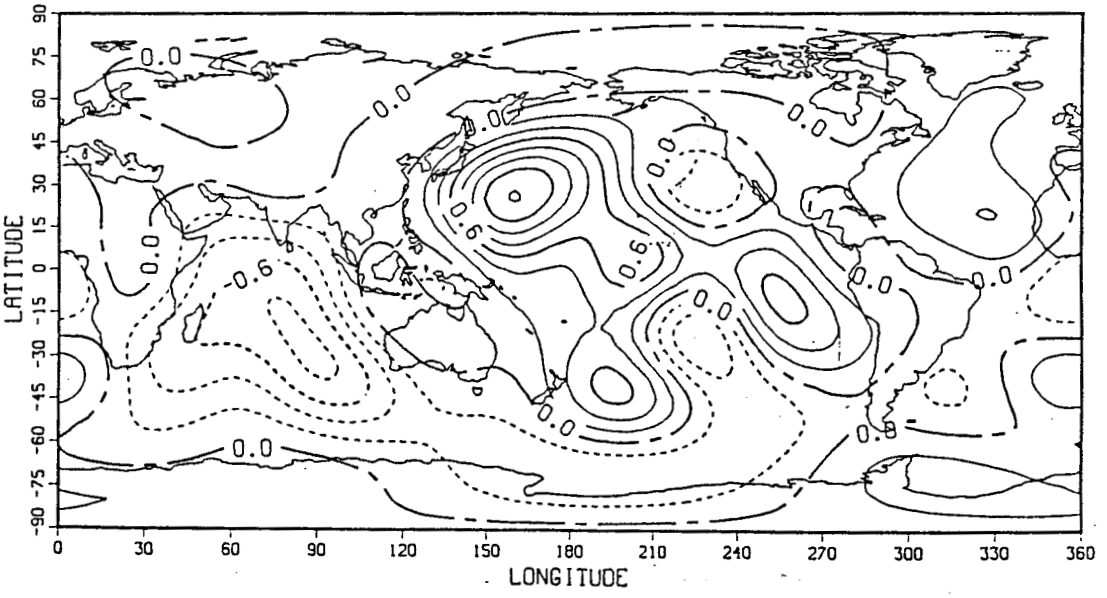

Fig. 2

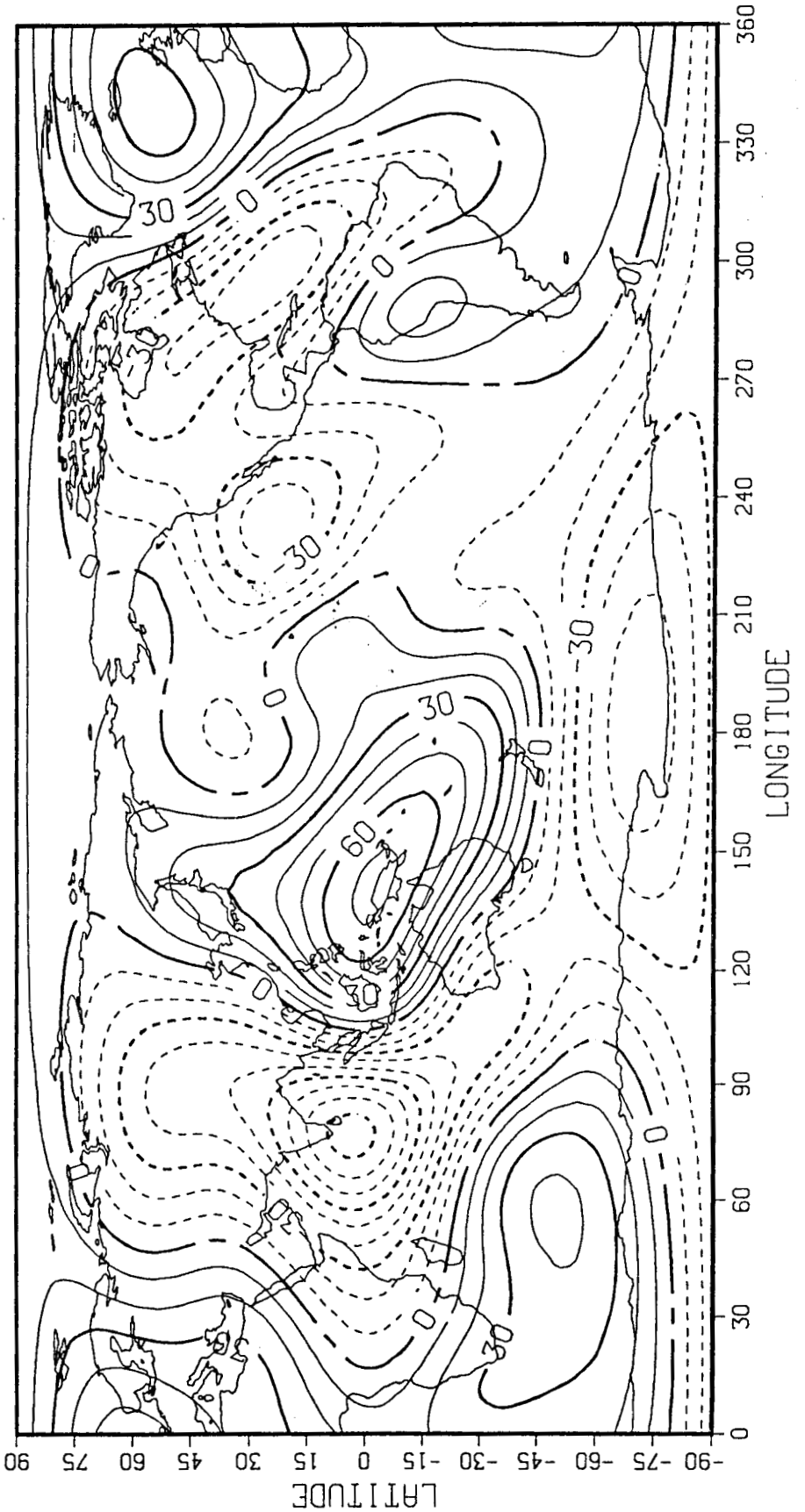

Fig. 3

(a)

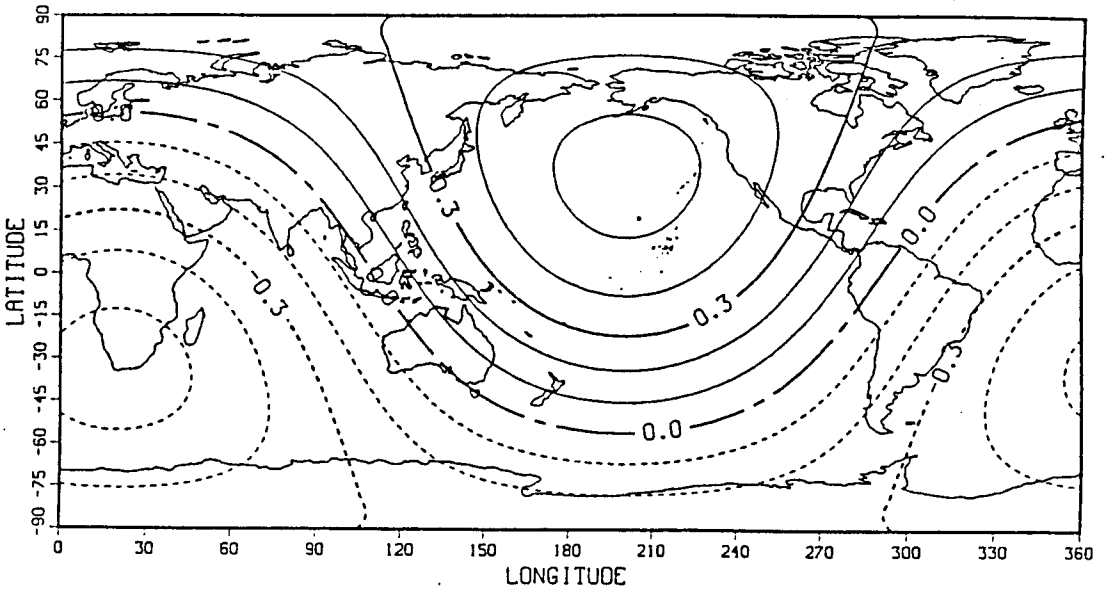

(b)

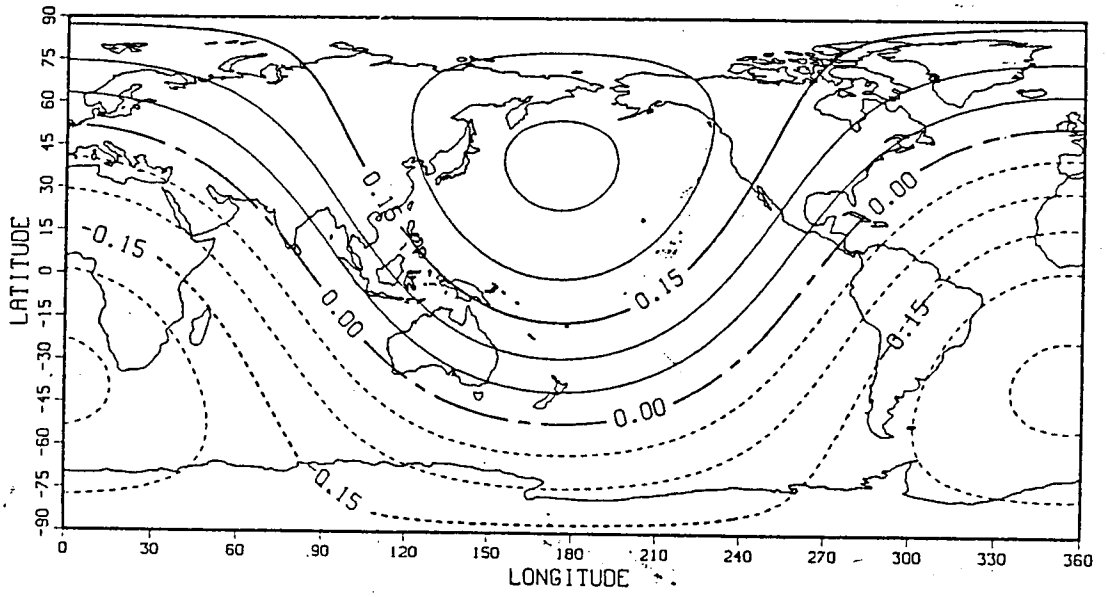

(c)

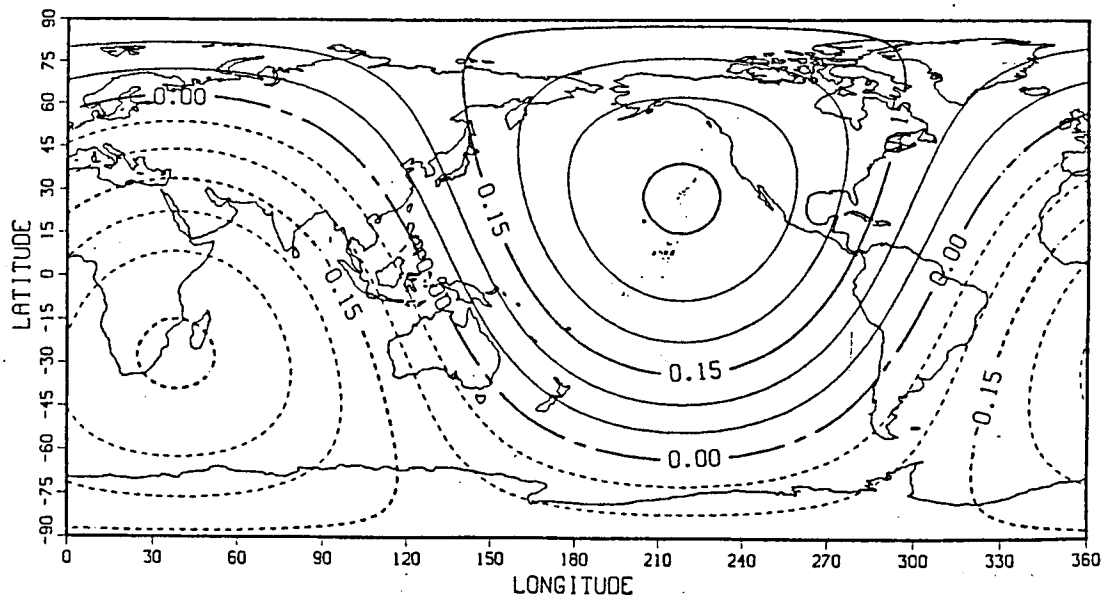

Fig. 4

(a)

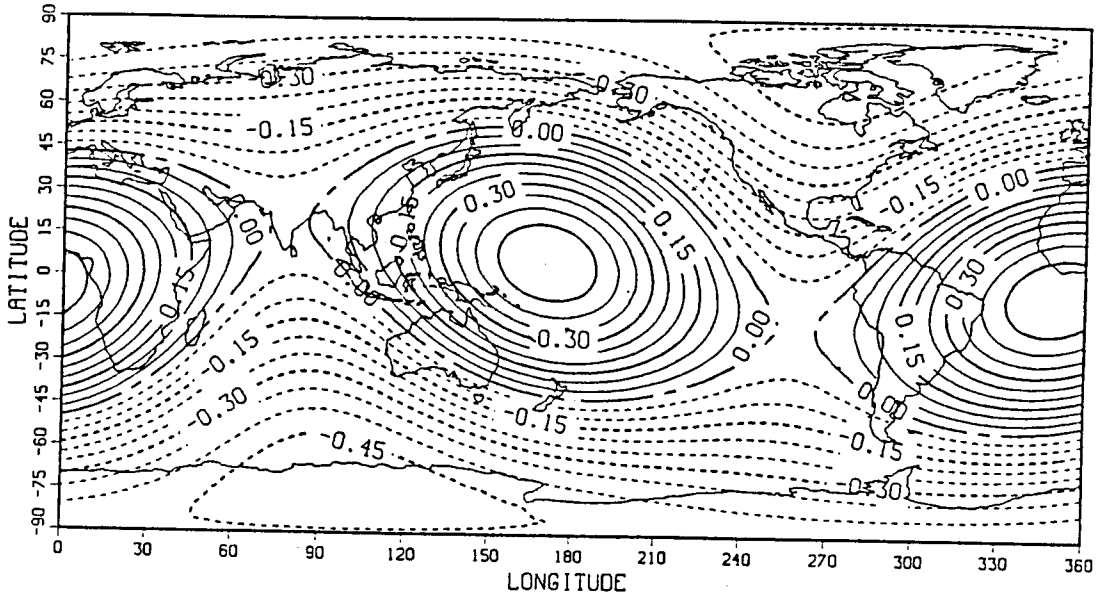

(b)

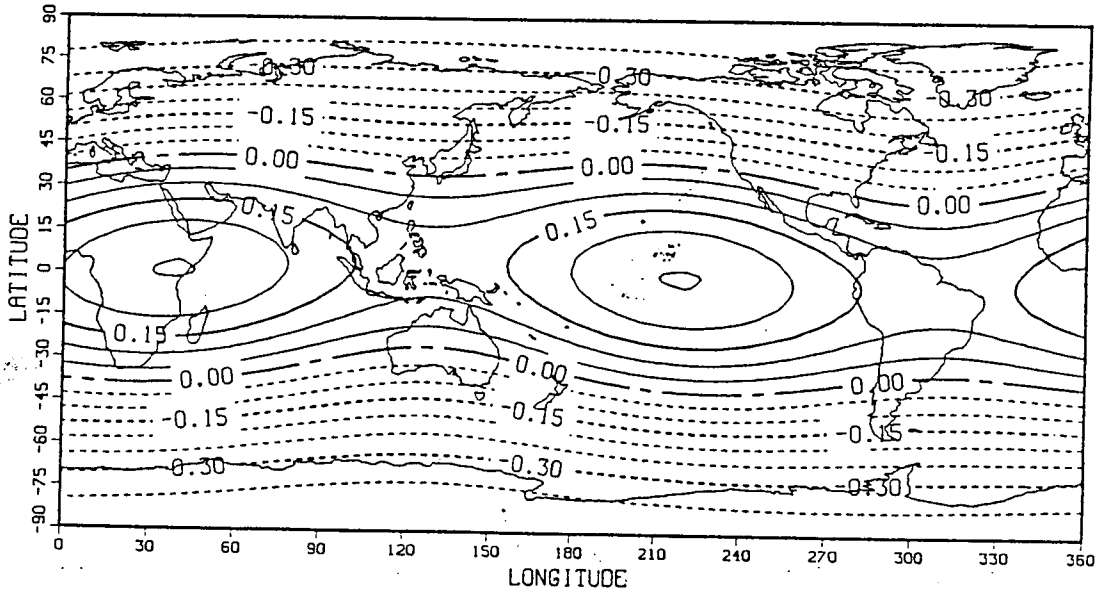

(c)

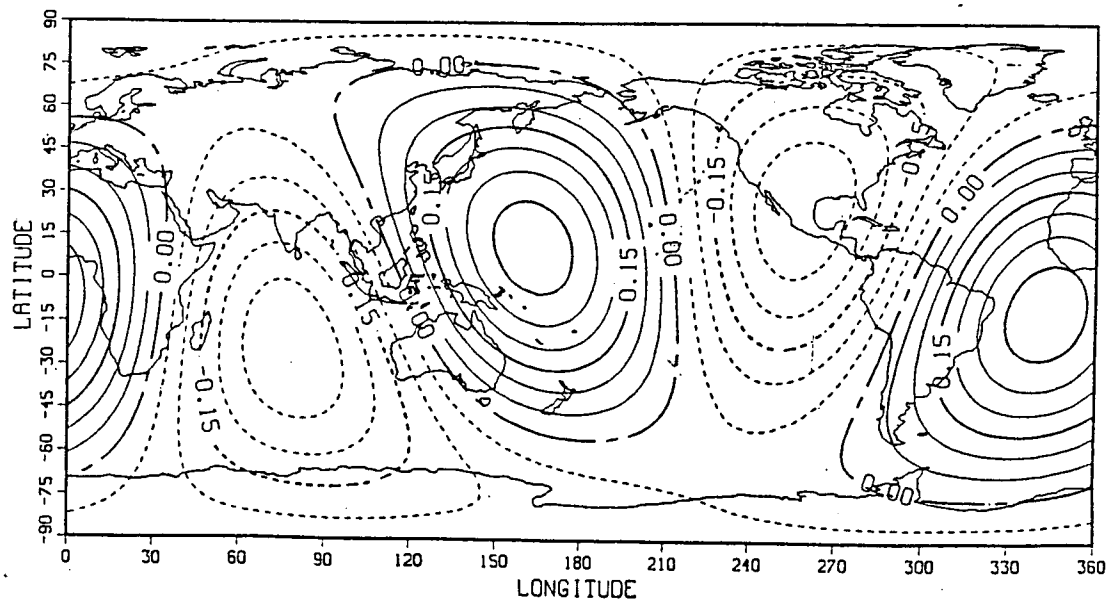

Fig. 5

(a)

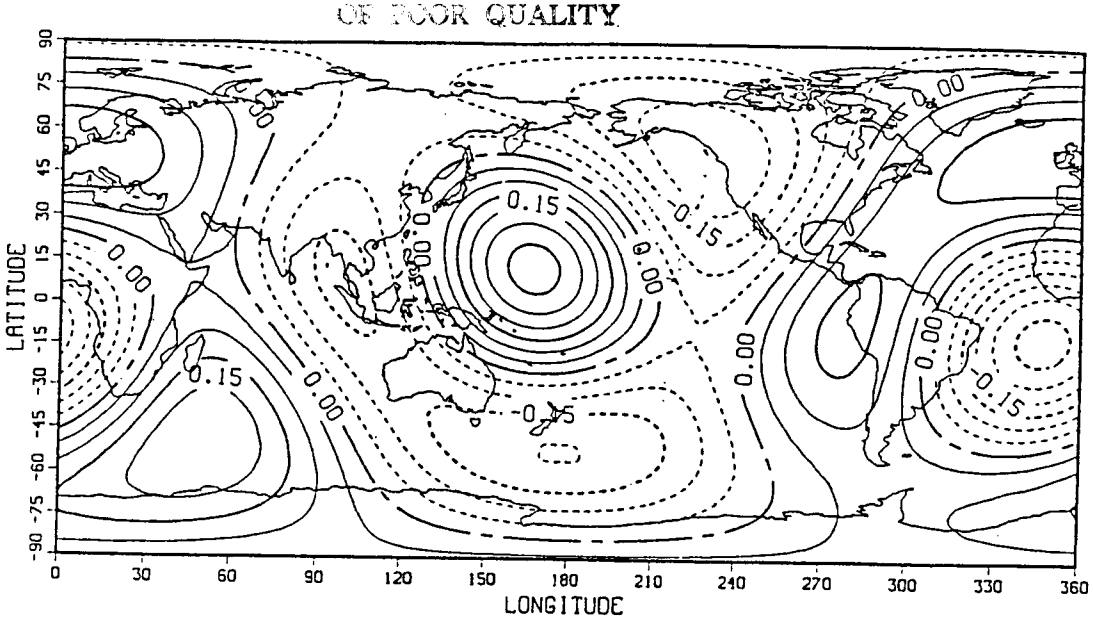

(b)

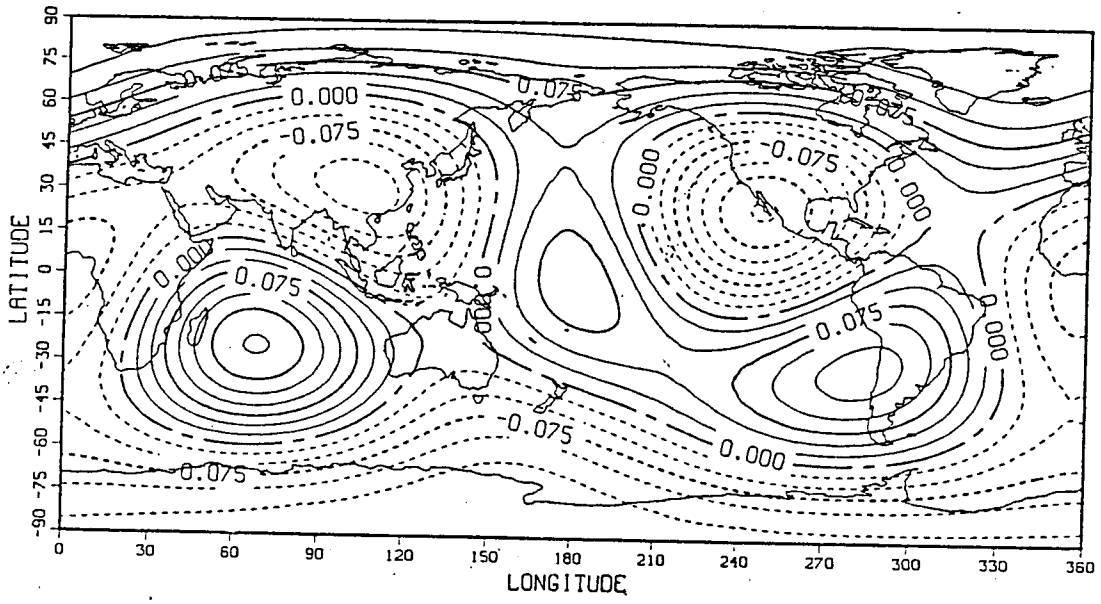

(c)

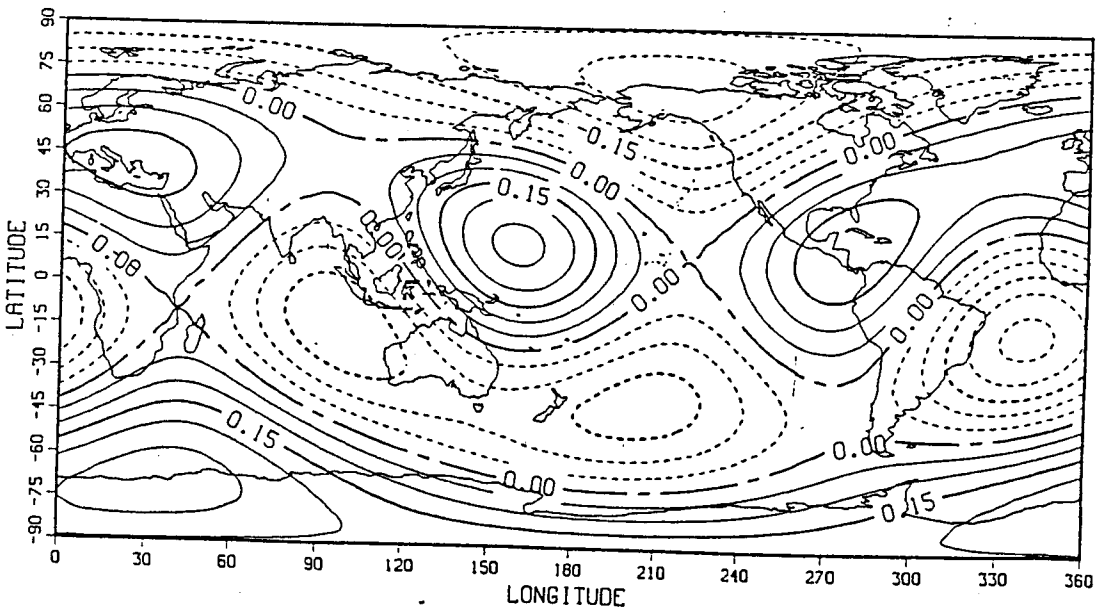

Fig. 6

(a)

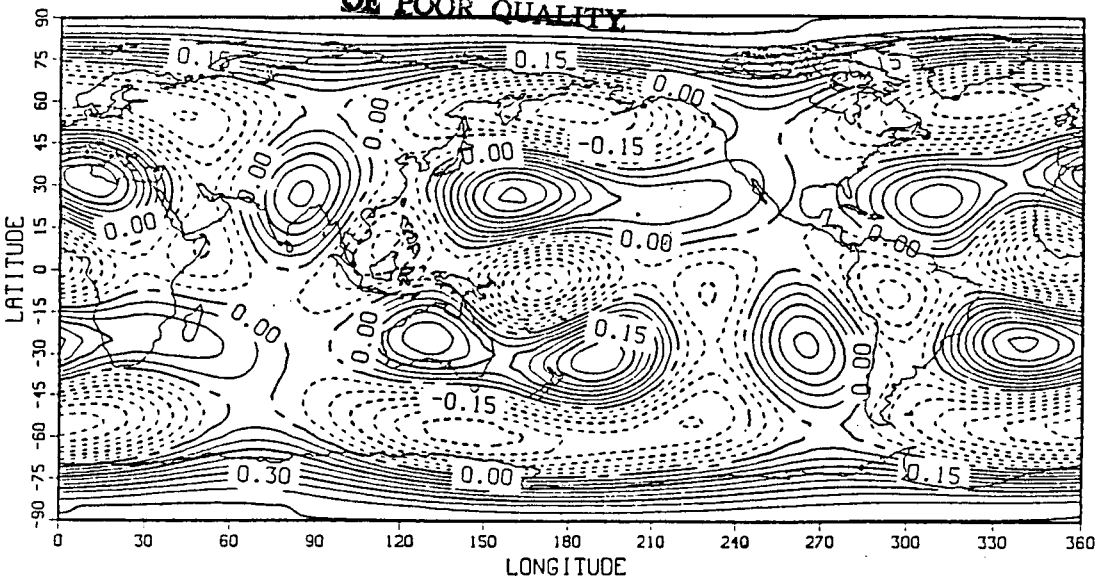

(b)

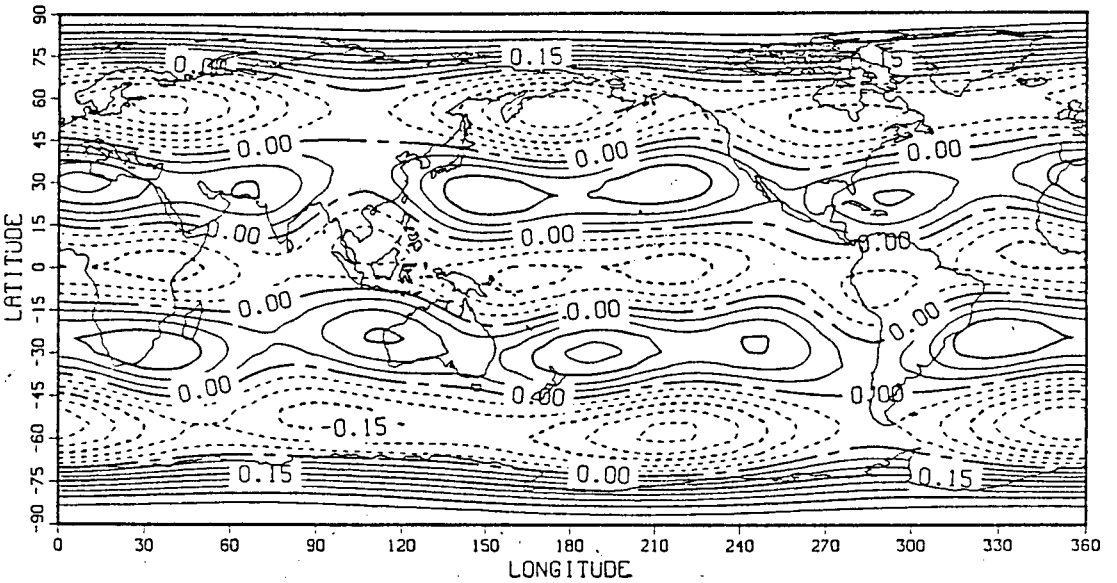

(c)

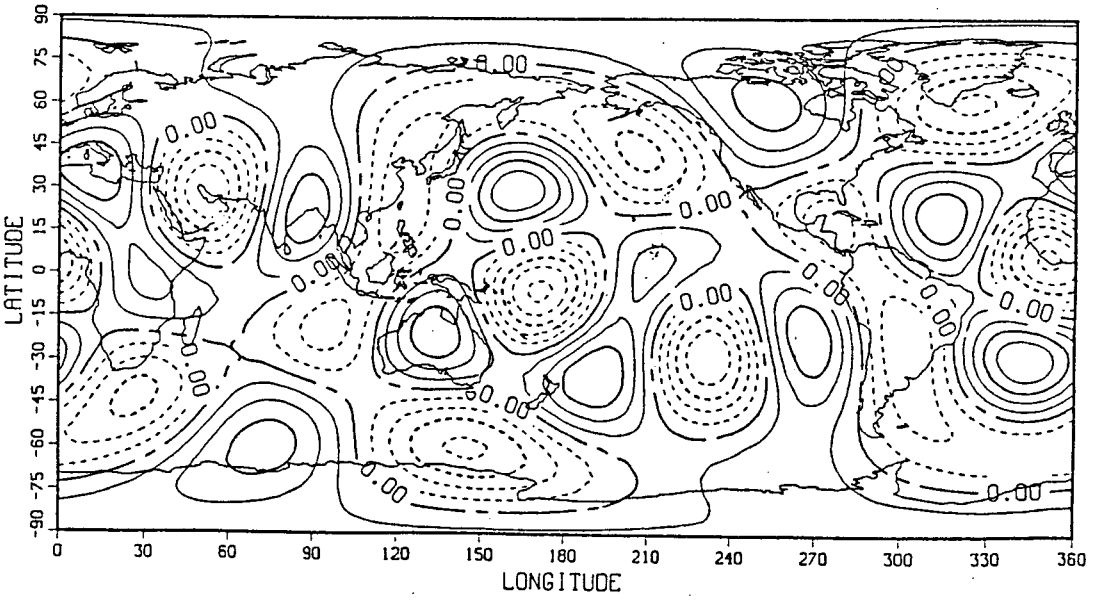

Fig. 7

Table 1

The meaning of the subscript

Subscript	Geoid Model		Procedure
a	GEM-T1		aliased, edge unsmoothed
u	GEM-T1		5° x 5° average, edge unsmoothed
1	GEM-T1		5° x 5° average, edge smoothed
2	GEM-L2		5° x 5° average, edge smoothed
3	GEM-L2 PGS-S4	degree 2-6 degree 7-36	5° x 5° average, edge smoothed
4	PGS-S4		5° x 5° average, edge smoothed
6	GEM-T1 PSG-S4	degree 2-6 degree 7-36	5° x 5° average, edge smoothed
8	GEM-T1 PGS-S4	degree 2-8 degree 9-36	5° x 5° average, edge smoothed

Table 2

Square roots of degree variances of the direct estimate, $\overline{D}$, in cm

Degree	$\overline{D_a}$	$\overline{D_u}$	$\overline{D_1}$	$\overline{D_2}$	$\overline{D_3}$	$\overline{D_4}$	$\overline{D_6}$	$\overline{D_8}$
1	36.85	36.48	30.91	30.01	30.22	32.50	30.65	31.00
2	30.51	29.60	25.04	30.04	26.80	26.28	25.05	25.64
3	14.45	13.63	13.20	13.35	14.41	10.53	13.46	13.09
4	10.63	10.48	10.41	16.00	11.37	11.98	7.69	8.43
5	13.71	13.51	11.80	12.78	12.36	7.48	11.75	11.97
6	19.83	19.02	17.68	21.35	20.22	16.06	16.90	17.16
7	14.07	13.63	13.02	20.01	13.28	12.64	11.73	13.02
8	13.85	13.34	9.90	14.07	7.67	8.26	7.90	11.48
9	12.29	12.33	9.76	18.48	5.85	5.95	6.02	6.12
10	17.37	16.86	13.47	21.38	9.09	8.57	9.27	9.43
0 - 6	56.49	55.19	48.32	53.79	50.42	48.25	47.36	48.08
0 - 8	59.85	58.39	51.01	59.09	52.70	50.56	49.42	51.12
9 - 20	59.78	56.68	47.19	85.49	24.78	23.24	24.29	24.70
21-36	73.45	58.97	47.68	64.65	26.85	26.66	26.81	26.89
0 - 36	112.0	100.5	84.28	122.4	64.13	61.71	61.25	62.81
37-90	93.86	46.80	27.91	29.50	26.06	26.12	26.12	25.98
0-90	146.1	110.9	88.78	125.9	69.21	67.01	66.59	67.98

Table 3

Square roots of degree variances of the discrepancy $\overline{F}$, in cm

Degree	$\overline{F_a}$	$\overline{F_u}$	$\overline{F_1}$	$\overline{F_2}$	$\overline{F_3}$	$\overline{F_4}$	$\overline{F_6}$	$\overline{F_8}$
1	21.85	21.71	18.11	18.39	17.17	19.18	17.54	17.72
2	19.85	18.84	15.71	22.63	18.63	18.92	16.21	16.24
3	14.99	14.03	12.65	11.28	12.64	11.59	13.16	12.25
4	10.29	10.50	9.78	14.46	10.48	11.91	7.89	7.87
5	12.84	12.50	10.49	10.68	10.36	8.34	10.60	10.27
6	12.30	11.99	11.26	17.12	12.97	8.48	9.32	9.93
7	7.42	7.10	7.53	18.06	8.65	8.64	7.66	7.86
8	9.52	9.09	7.00	13.19	7.32	7.04	7.26	8.42
9	12.59	12.71	10.75	19.19	6.52	6.54	6.41	6.63
10	17.25	16.77	12.64	21.59	7.96	7.85	8.02	7.95
0 - 6	38.97	37.86	32.90	40.32	34.59	33.97	31.83	31.68
0 - 8	40.80	39.58	34.47	46.11	36.40	35.75	33.54	33.71
9-20	58.86	55.81	46.69	84.85	23.52	22.49	22.85	22.91
21-36	72.67	58.04	47.48	64.76	26.46	26.31	26.38	26.48
0-36	102.0	89.72	74.98	116.3	50.77	49.76	48.40	48.60
37-90	92.79	44.94	27.46	28.98	25.98	26.10	26.02	25.92
0-90	137.9	100.4	79.85	119.8	57.04	56.19	54.85	55.08

Table 4

Square roots of degree variance of Levitus' dynamic topography (0-2250 db), $\overline{\hat{\eta}}$, in cm

Degree	$\overline{\hat{\eta}_a}$ (aliased, edge unsmoothed)	$\overline{\hat{\eta}_u}$ (5° x 5° average, edge unsmoothed)	$\overline{\hat{\eta}}$ (5° x 5° average, edge smoothed)
1	17.82	17.83	15.00
2	21.87	21.83	17.13
3	9.18	9.13	7.46
4	7.19	7.21	6.77
5	7.17	7.17	6.51
6	13.57	13.51	12.05
7	10.70	10.65	9.50
8	7.83	7.74	5.97
9	5.53	5.42	3.87
10	3.00	2.97	2.80
0-6	34.17	34.11	28.42
0-8	36.65	36.56	30.56
9-20	13.64	13.45	11.76
21-36	10.05	9.90	6.40
0-36	40.38	40.20	33.36
37-90	12.61	12.49	5.10
0-90	42.30	42.10	33.75

Table 5

Square roots of degree variances of $\delta\hat{N}_1$, (i.e., the uncertainty estimates of GEM-T1), $\hat{N}_1-\hat{N}_2$ (i.e., GEM-L2), $\hat{N}_1-\hat{N}_4$ (i.e., PGS-S4), and $\hat{N}_2-\hat{N}_4$, in cm

Degree	$\delta\hat{N}_1$	x.4795	$\hat{N}_1-\hat{N}_2$	x.4795	$\hat{N}_1-\hat{N}_4$	x.4795	$\hat{N}_2-\hat{N}_4$	x.4795
2	0.0	0.0	2.21	1.06	12.52	6.00	13.26	6.36
3	1.56	0.75	3.51	1.68	11.44	5.49	13.62	6.53
4	2.47	1.18	8.36	4.01	11.27	5.40	16.08	7.71
5	4.93	2.36	7.96	3.82	15.24	7.31	15.33	7.35
6	4.93	2.36	15.69	7.52	13.94	6.68	18.68	8.96
7	8.03	3.85	24.88	11.93	22.46	10.77	32.48	15.57
8	9.45	4.53	20.16	9.67	14.29	6.85	15.65	7.50
9	14.27	6.84	28.97	13.89	24.19	11.60	36.07	17.30
10	14.17	6.79	33.56	16.09	31.44	15.08	36.08	17.30
2-6	7.57	3.63	19.91	9.55	29.01	13.91	34.70	16.64
2-8	14.53	6.97	37.71	18.08	39.37	18.88	50.04	23.99
9-20	87.70	42.05	156.6	75.09	124.7	59.79	175.1	83.96
21-36	129.8	62.24	124.4	59.65	144.4	69.24	160.4	76.91
2-36	157.3	75.43	203.5	97.58	194.8	93.41	242.7	116.4

Table 6

Pattern correlation between $\overline{\hat{\eta}}$ and a variety of $\overline{D}$

Degree	$\overline{D}_1$	$\overline{D}_2$	$\overline{D}_3$	$\overline{D}_4$	$\overline{D}_6$	$\overline{D}_8$
1	0.919	0.874	0.930	0.937	0.932	0.938
2	0.785	0.664	0.724	0.695	0.767	0.782
3	0.354	0.535	0.482	0.204	0.317	0393
4	0.415	0.428	0.424	0.293	0.410	0.482
5	0.467	0.551	0.545	0.296	0.446	0.515
6	0.777	0.598	0.792	0.856	0.845	0.825
7	0.821	0.433	0.760	0.730	0.759	0.800
8	0.716	0.354	0.445	0.551	0.480	0.704
9	- 0.070	-0.085	0.147	0.165	0.217	0.179
10	0.392	-0.010	0.534	0.411	0.568	0.634
0-6	0.752	0.682	0.752	0.724	0.758	0.775
0-8	0.755	0.639	0.742	0.717	0.746	0.773

Table 7

Summary of the result based on $\hat{N}_8$

Degree	$\overline{D}_8$	$\overline{F}_8$	$\overline{\hat{\eta}}$	Pattern Correlation	Error Estimates for GEM-T1	x.4795
1	31.00	17.72	15.00	0.938	N.A.	N.A.
2	25.64	16.24	17.13	0.782	0.0	0.0
3	13.09	12.25	7.46	0.393	1.56	0.75
4	8.43	7.87	6.77	0.482	2.47	1.18
5	11.97	10.27	6.51	0.515	4.93	2.36
6	17.16	9.93	12.05	0.825	4.93	2.36
7	13.02	7.86	9.50	0.800	8.03	3.85
8	11.48	8.42	5.97	0.704	9.45	4.53
9	6.12	6.63	3.87	0.179	14.27	6.84
10	9.43	7.95	2.80	0.634	14.17	6.79
0-6	48.08	31.68	28.42	0.775	7.57	3.63
0-8	51.12	33.71	30.56	0.773	14.53	6.97